Laminar Chaos in Experiments: Nonlinear Systems with Time-Varying Delays and Noise

Joseph D. Hart, Rajarshi Roy, David Müller-Bender, Andreas Otto, and Günter Radons

Laminar Chaos in experiments: Nonlinear systems with time-varying delays and noise

Joseph D. Hart,[1, 2, *] Rajarshi Roy,[1, 2, 3, †] David Müller-Bender,[4, ‡] Andreas Otto,[4, §] and Günter Radons[4, ¶]

[1]*Institute for Research in Electronics and Applied Physics,*
University of Maryland, College Park, Maryland 20742, USA
[2]*Department of Physics, University of Maryland, College Park, Maryland 20742, USA*
[3]*Institute for Physical Science and Technology, University of Maryland, College Park, Maryland 20742, USA*
[4]*Institute of Physics, Chemnitz University of Technology, 09107 Chemnitz, Germany*
(Dated: August 28, 2019)

A new type of dynamics called Laminar Chaos was recently discovered through a theoretical analysis of a scalar delay differential equation with time-varying delay. Laminar Chaos is a low-dimensional dynamics characterized by laminar phases of nearly constant intensity with periodic durations and a chaotic variation of the intensity from one laminar phase to the next laminar phase. This is in stark contrast to the typically observed higher-dimensional Turbulent Chaos, which is characterized by strong fluctuations. In this paper we provide the first experimental observation of Laminar Chaos by studying an opto-electronic feedback loop with time-varying delay. The noise inherent in the experiment requires the development of a nonlinear Langevin equation with variable delay. The results show that Laminar Chaos can be observed in higher-order systems, and that the phenomenon is robust to noise and a digital implementation of the variable time-delay.

Time delays, typically due to the finite propagation speed of signals, can be found in models of lasers [1–3], control systems [4, 5], population dynamics [6], immune diseases [7], and networks of neurons [8, 9]. Systems with time delays are known to display a wide variety of interesting dynamical behaviors, including square waves [10] and multistability [11, 12], and have even been shown to exhibit spatio-temporal-like behaviors such as phase transitions [13], coarsening [14], and chimera states in ring networks [15] and arbitrary networks [16, 17] when viewed in the space-time representation [18]. Time delay systems have long been known for their ability to display high-dimensional chaotic behavior [19]. Recent developments in the field of time delay systems can be found in the theme issue [20].

Most previous studies of time-delay systems have considered systems with a fixed time delay. Less understood is the case in which the duration of the delay itself is allowed to vary in time. This possibly more realistic case can lead to an increase in dynamical complexity [21, 22], or alternatively a stabilization of the system [23, 24]. Only a few experiments (notable ones include the electronic circuits described in Refs. [25] and [26]) have been performed with tunable time-varying delays. Here, we develop the first opto-electronic oscillator with time-varying delay.

In 2018 an entirely new type of chaos, *Laminar Chaos*, was discovered in a scalar time-delay system with a varying delay [27]. In this Letter, we report an opto-electronic oscillator that displays Laminar Chaos, the first observation of Laminar Chaos in an experiment. Our results demonstrate that Laminar Chaos can be observed in higher-order systems with a digital implementation of the variable delay. Further, we study the robustness of Laminar Chaos to noise, both in the experiment and in a nonlinear Langevin equation with variable delay.

In Ref. [27] Laminar Chaos was found in systems described by a scalar delay differential equation with time-varying delay $\tau(t)$

$$\frac{1}{T}\dot{z}(t) + z(t) = \mu\, F(z(t - \tau(t))), \qquad (1)$$

Equation (1) describes a first-order (one-pole) low-pass filter with nonlinear time-delayed feedback in which the duration of the delay varies in time. In Eq. 1, z is a generic dependent variable, $F(z)$ is a generic nonlinearity, $T/2\pi$ is the cutoff frequency of the low-pass filter, and $\tau(t)$ is the time-varying time delay. In Eq. 1, time is dimensionless. Equation (1) contains the essential ingredients for Laminar Chaos: a feedback loop with a band-limiting element (low pass filter), a nonlinearity $F(z)$, and a time-varying time delay $\tau(t)$. A block diagram depicting such a system is given in Fig. S1 (Supplemental Material).

Laminar Chaos is characterized by nearly constant laminar phases with periodic durations and burst-like transitions between them. The intensity levels z_n of the laminar phases vary chaotically and are connected by the one dimensional map $z_{n+1} = F(z_n)$. The durations of the phases are determined by the so-called access map $t_{n+1} = R(t_n) \equiv t_n - \tau(t_n)$ [27]. In other words, a system that is well-described by a continuous-time delay differential equation displays essentially discrete-time dynamics described by a chaotic map.

In order to study Laminar Chaos in an experiment, we use an opto-electronic oscillator. An opto-electronic oscillator is an attractive system for the study of Laminar Chaos because it is a well-understood system whose oscillations arise from nonlinearity and time delayed feedback. Opto-electronic oscillators with fixed time delays have been used for a variety of applications, including generation of microwaves with low phase noise [28, 29], neuromorphic computing [30, 31], sensing [32],
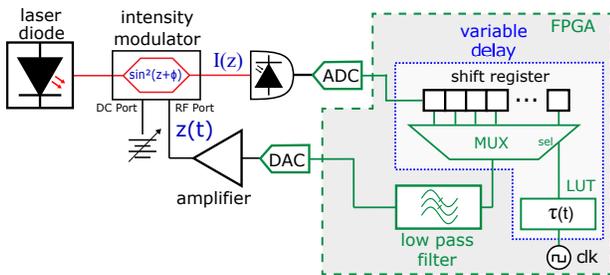
FIG. 1. An illustration of the opto-electronic oscillator we used to observe Laminar Chaos. Red lines indicate the optical path, black lines indicate the electronic path, and green lines indicate signal-processing on the FPGA.

and chaotic communications [33]. Opto-electronic oscillators are known to display a wide variety of dynamics [34–36], including periodic dynamics [28], breathers [37] and broadband chaos [38].

An illustration of our opto-electronic oscillator is shown in Fig. 1. A fiber-coupled laser diode emits light at a constant intensity. The light intensity is modulated by an integrated Mach-Zehnder intensity modulator such that the normalized intensity transmitted through the modulator is given by $I(z) = \sin^2(z(t) + \phi)$ where $z(t)$ is the normalized voltage applied to the RF port of the modulator and ϕ is the modulator bias. The modulator provides the nonlinearity in our feedback loop; i.e., in our system $F(z) = \sin^2(z(t) + \phi)$. The output of the modulator is converted into an electrical signal by a DC-coupled photoreceiver. This electrical signal is read into a field-programmable gate array (FPGA) via an analog-to-digital converter (ADC). The time-varying delay is implemented via a tapped shift-register and multiplexer (MUX) on the FPGA. The output of the variable delay is digitally filtered by a second-order (two-pole Butterworth) low pass filter with cutoff frequency $f_{\text{cut}} = 3183$ Hz. The filtered signal is output via a digital-to-analog converter (DAC). This electrical signal is amplified and applied to the RF port of the modulator, completing the feedback loop. The round-trip gain of the feedback loop is quantified by the parameter μ. We measure μ directly by breaking the feedback loop at the input to the modulator and measuring the steady-state value of z.

While the FPGA gives us great flexibility in the choice of the form of the delay $\tau(t)$, we choose the time-varying delay as

$$\tau(t) = \tau_0 + \frac{A}{2\pi} \sin(2\pi t/\tilde{T}), \qquad (2)$$

where τ_0, A and $\tilde{T}$ are the mean, amplitude and period of the delay, respectively. The FPGA is clocked at a frequency ν_s and thus operates in discrete time. We choose $\nu_s = 100 \, \text{kHz}$ and the delay period $\tilde{T} = 10 \, \text{ms}$, so that one period of the delay is divided into 1000 time steps. Thus, Eq. (2) is an accurate approximation of the piecewise-

continuous variation of the delay in the experiment. Table S1 in the Supplemental Material provides a list of the parameter values that describe our opto-electronic oscillator as well as the corresponding parameters in dimensionless time such that the period of the delay $\tilde{T} = 1$, which are used for numerical simulations.

There are two fundamentally different classes of time-varying delays [39, 40]. Systems with conservative delays are equivalent to systems with constant delay; on the other hand, systems with dissipative delays (that is, the access map $t_{n+1} = R(t_n)$ is dissipative) are not. Only systems with dissipative delays are candidates to display Laminar Chaos [27]. We consider two different values of the parameter τ_0 so that we can explore our opto-electronic oscillator with a dissipative delay ($\tau_0 = 15.0$ ms) and with a conservative delay ($\tau_0 = 15.4$ ms). In Ref. [27] it was shown that a further necessary condition for Laminar Chaos is given by $\lambda[F] > 0$ and

$$\lambda[F] + \lambda[R] < 0, \qquad (3)$$

where $\lambda[F]$ and $\lambda[R]$ are the Lyapunov exponents of the map $z_{n+1} = F(z_n)$ and the access map $t_{n+1} = R(t_n)$, respectively. For our system, $\lambda[R] \approx -0.83$ when $\tau_0 = 15.0$ ms (and $\lambda[R] = 0$ when $\tau_0 = 15.4$ ms). We choose $\mu = 2.2$ and $\phi = \frac{\pi}{4}$ so that $\lambda[F] \approx 0.31$ and Eq. 3 is satisfied when $\tau_0 = 15.0$ ms.

Noise plays an important role in any experimental system. In our opto-electronic setup, inherent sources of noise include discretization noise in the ADC and DAC, electronic noise in the DAC amplifier, and Johnson noise in the photoreceiver. In order to experimentally test the robustness of Laminar Chaos to different amounts of noise, we use the FPGA to add noise to the experiment in a controlled way. Specifically, at each time step we add numerically generated Gaussian white noise with zero mean and standard deviation ζ to the normalized intensity I measured by the ADC.

Figure 2 shows measured experimental time series. When $\tau_0 = 15.0$ ms, the delay is dissipative and Laminar Chaos is observed, as shown in Figure 2a-c for different values of added noise strength ζ. The nearly constant laminar phases are clear in Fig. 2a-b, but are more difficult to observe by inspection in Fig. 2c. In contrast, when we set $\tau_0 = 15.4$ ms, the delay becomes conservative and we observe only Turbulent Chaos (Fig. 2d-e).

Our opto-electronic oscillator possesses the three main attributes–a nonlinearity, a band-limiting element, and a time-varying delay–that are modeled by Eq. 3 and are necessary for Laminar Chaos [27]. However, there are three significant differences between the present experimental realization and the theoretical investigation in Ref. [27]. First, we used a two-pole Butterworth filter, which means that our opto-electronic oscillator is a second-order system. Second, the ADC and DAC induce digitization ("sampling") and quantization ("round-off") noise into the experiment, which may have significant
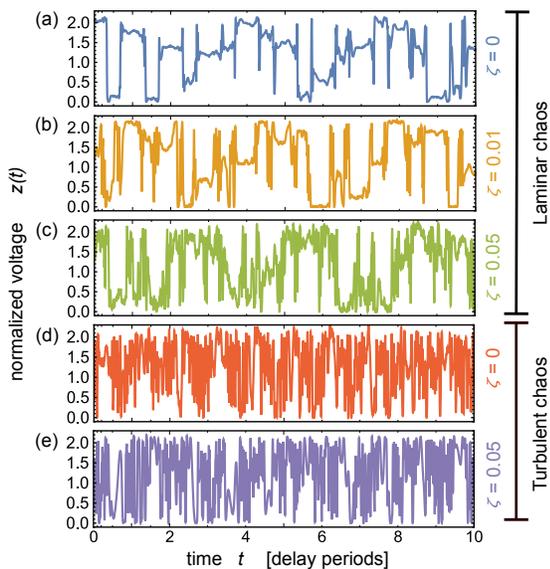
FIG. 2. Experimental time-series for different values of the mean delay τ_0 and for different values of the strength ζ of the external noise. The trajectories $(a) - (c)$ correspond to a dissipative delay ($\tau_0 = 15.0\,\text{ms}$) and show Laminar Chaos, whereas the trajectories (d) and (e) correspond to a conservative delay ($\tau_0 = 15.4\,\text{ms}$) and show Turbulent Chaos.

FIG. 3. Trajectories generated from Eq. (4) with parameters from Table S1 for different mean delays τ_0 and noise strengths σ. The trajectories $(a) - (c)$ correspond to a dissipative delay ($\tau_0 = 1.5$) and show Laminar Chaos, whereas the trajectories (d) and (e) correspond to a conservative delay ($\tau_0 = 1.54$) and show Turbulent Chaos.

effects on the dynamics of hybrid systems with delayed feedback ([41, 42] and Refs. therein). The effect of a digital implementation on the access map dynamics is not clear, but the experimental results show that Laminar Chaos can still be observed. Third, noise is present in the experiments, which can make it difficult to identify laminar phases for increasing noise strength. In the following, we study the robustness of Laminar Chaos to noise and show that the noisy trajectories (a)-(c) exhibit features that clearly distinguish Laminar Chaos from other dynamics. All together, our results show that Laminar Chaos is robust to the details of the experimental implementation and therefore should be possible in a variety of natural and engineered systems.

In order to take into account the presence of noise in the general model of Laminar Chaos (Eq. 1), we consider the following delayed Langevin equation

$$\frac{1}{T}\dot{z}(t) + z(t) = \mu\,F(z(t - \tau(t))) + \frac{\sigma}{\sqrt{T}}\,\xi(t). \quad (4)$$

Exemplary trajectories of Eq. (4) for dimensionless parameters as in Table S1 are shown in Fig. 3. The trajectories in Fig. 3a-c were computed with $\tau_0 = 1.5$, while those in Fig. 3d-e were computed with $\tau_0 = 1.54$. In all cases, the trajectories give qualitative agreement with the corresponding experimental time series in Fig. 2.

Two identifying features of Laminar Chaos are the periodicity of the duration of the laminar phases, which is equal to the delay period [27], and the description of the intensity levels of the laminar phases by a one-
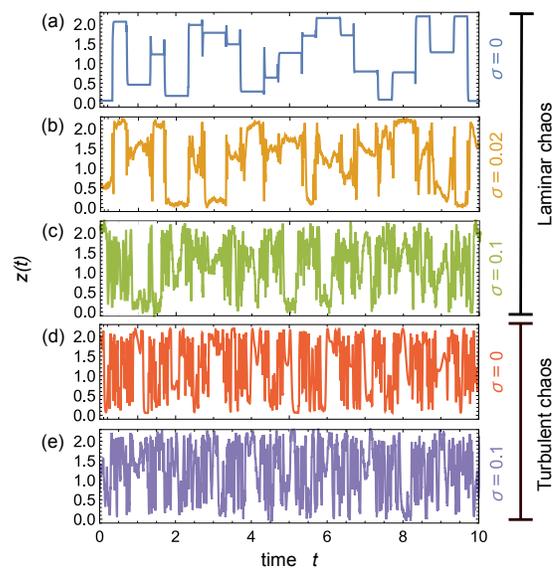
dimensional chaotic map $z_{n+1} = F(z_n)$. We now show that these features can be used to identify Laminar chaos in the time series from our opto-electronic experiment and from simulations of Eq. (4). The laminar phases can be validated by considering the derivative of z. Without noise ($\sigma = 0$), the derivative is roughly zero between the bursts, i.e., it is characterized by phases with approximately zero amplitude, which are periodically interrupted by short large amplitude bursts. In the presence of noise we consider the approximate derivative $\Delta_h[z](t) = \frac{z(t+h)-z(t)}{h}$ instead of the derivative, since the latter is not well defined. In this case the approximate derivative is characterized by phases of small amplitude which are periodically interrupted by short large amplitude bursts. For increasing noise strength σ, one expects that the fluctuation strength in the low amplitude phases increases, such that the periodic structure is still present but gets blurred. To determine the position of the laminar phases of a laminar chaotic trajectory $z(t)$, we consider the temporal distribution of the variance $\sigma_d^2[z](t)$ of the approximate derivative $\Delta_h[z](t)$, which is defined by

$$\sigma_d^2[z](t) = \lim_{N\to\infty} \frac{1}{N} \sum_{n=0}^{N-1} \left(\Delta_h[z](t + n\tilde{T})\right)^2 - (\mu_d[z](t))^2, \quad (5)$$

where

$$\mu_d[z](t) = \lim_{N\to\infty} \frac{1}{N} \sum_{n=0}^{N-1} \Delta_h[z](t + n\tilde{T}). \quad (6)$$

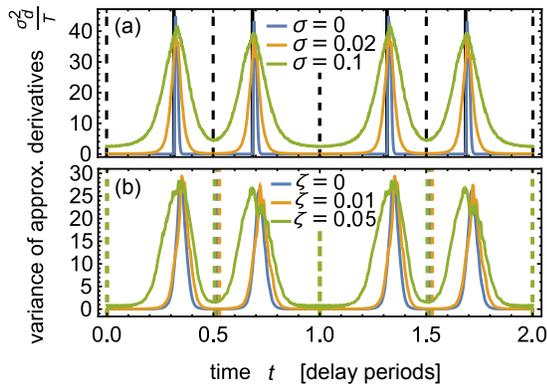If the delay period $\tilde{T}$ is unknown, it can be determined

FIG. 4. Detection of the laminar phases: Temporal distribution of the variance σ_d^2 (in units of $\frac{T}{h}$) of the approximate derivatives ($h \approx 0.0033$) of (a) laminar chaotic trajectories of Eq. (4) and (b) experimental trajectories (same parameters as in Fig. 2 and Fig. 3). The laminar phases (low σ_d^2) and the burst-like transitions between them (high σ_d^2) are located around the attractive and repulsive fixed points of the reduced access map (dashed and solid lines in (a)), respectively. In the experimental data the location of the attractive fixed point is not known, and approximated via the local minima of σ_d^2 (dashed lines in (b)). The rotation number ρ of the access map is $\rho = -\frac{3}{2}$ leading to $q = 2$ laminar phases per period.
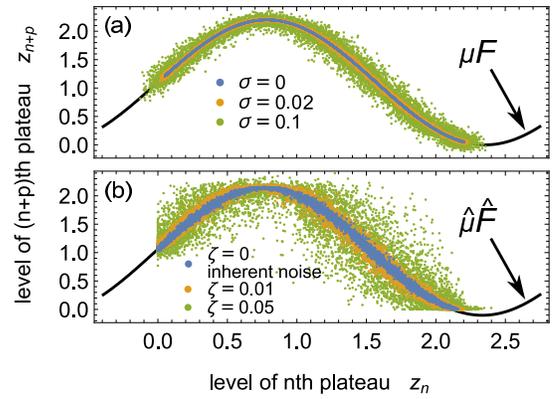

FIG. 5. Connection between the laminar phases for the laminar chaotic trajectories from (a) Fig. 3 (simulation) and (b) Fig. 2 (experiment). The intensity $z_{n+p'}$ of the $(n+p')$th laminar phase is plotted vs. the intensity z_n of the nth phase for $p = p' = 3$. The reconstruction of the nonlinearity $(z, \mu F(z))$ (solid line) is possible even for high noise strengths. For the experimental data the black line represents the fit of the data for $\zeta = 0$ to the nonlinearity $\hat{\mu}\hat{F}(z) = \hat{\mu}\sin^2(z + \hat{\phi}_0) + \hat{c}_0$, where $\hat{\mu} \approx 2.229 \pm 0.002$, $\hat{\phi}_0 \approx 0.8074 \pm 0.0004$ and $\hat{c}_0 \approx -0.103 \pm 0.002$, where the $\hat{\ }$ is used to emphasize that the these parameter values are fits to the data shown in Fig. 5b, not directly measured. The clipping below $z = 0$ is due to the fact that the light intensity cannot be lower than zero.

by analyzing the power spectrum of $\Delta_h[z]$, in which there are large peaks at integer multiples of $1/\tilde{T}$.

Figure 4 shows the variance σ_d^2 of exemplary Laminar Chaos trajectories generated with different noise strengths σ and ζ via Eq. (4) (a) and via the experimental setup (b). The periodic alternation of high and low values of σ_d^2 corresponds to high (bursts) and low frequency (laminar) phases of the laminar chaotic trajectory. The local minima of σ_d^2 can be used to determine the position of the laminar phases and the number of laminar phases per period, i.e. the denominator q of the rotation number of the access map.

Next, we check the connection of the intensity levels of nearby laminar phases, i.e., the connection between the values of the trajectory at the local minima of σ_d^2. To do this, we plot the intensity $z_{n+p'}$ of the $(n+p')$th laminar phase against the intensity z_n of the nth laminar phase, where $p' \in \mathbb{N}$ and $p' > 0$. Define p as the numerator of the rotation number $\rho = -\frac{p}{q}$ of the access map R. For Laminar Chaos, when $p' = p$, the points (z_n, z_{n+p}) resemble the graph $(z, \mu F(z))$. If the access map is not known, one finds the correct $p' = p$ from the smallest number for which the points $(z_n, z_{n+p'})$ resemble a line, which means that both the nonlinearity $F(z)$ and the rotation number $\rho = -\frac{p}{q}$ of the access map can be reconstructed from laminar chaotic trajectories. If no such p' can be found, the trajectory can not be characterized as Laminar Chaos.

We observed exactly this behavior in numerical simu-

lations of Eq. 4 and experimental measurements. Fig. 5 shows the accurately reconstructed nonlinearity for $p' = p = 3$. This type of time series analysis can distinguish laminar chaos from both turbulent chaos and from the periodic square wave solutions described in Refs. [36] and [44]. For the turbulent chaos in Figs. 2d-e and 3d-e, the graph (not shown) of $(z_n, z_{n+p'})$ does not resemble a line for any p'; instead the entire space $z_n \in [0, \mu]$, $z_{n+p'} \in [0, \mu]$ is filled. In contrast, for a periodic square wave a similar plot would result in only two (or period doubled) points along the $\sin^2$ curve, rather than the full curve as in Fig. 5. Since we observe both the predicted periodicity of the temporal duration of the laminar phases and the relation of the amplitudes by the nonlinearity F, we can conclusively state that we have observed Laminar Chaos in our opto-electronic oscillator.

We have provided the first experimental demonstration of Laminar Chaos and confirmed its robustness to noise both experimentally and numerically. Our experiments show that a fundamentally new type of dynamical behavior exists in the real world, despite the highly sensitive nature of the access map dynamics and in the presence of noise, imperfections, and the hybridization of analog and digital components. This experimental observation stimulated the development of time series analysis techniques to show conclusively that we have observed laminar chaos and to distinguish it from other dynamical behaviors, such as turbulent chaos and period-doubled

square waves. Our work will motivate theoretical and experimental research to explore the world of phenomena opened up by the presence of time-varying delays. For example, the complex transition from laminar chaos to turbulent chaos via the sequence of generalized laminar chaos of increasing order [43] is not yet explored at all in experiments, and only partially in theoretical studies. Further, our experiments make clear the practical relevance of laminar chaos, and open up potential applications of its inherent time-multiplexing for communications and computing.

* jdhart12@gmail.com
† rroy@umd.edu
‡ david.mueller@physik.tu-chemnitz.de
§ otto.a@mail.de
¶ radons@physik.tu-chemnitz.de

[1] K. Ikeda, Opt. Commun. **30**, 257 (1979).
[2] K. Ikeda, H. Daido, and O. Akimoto, Phys. Rev. Lett. **45**, 709 (1980).
[3] R. Lang and K. Kobayashi, IEEE J. of Quantum Electron. **16**, 347 (1980).
[4] G. F. Franklin, J. D. Powell, A. Emami-Naeini, and J. D. Powell, *Feedback control of dynamic systems*, Vol. 3 (Addison-Wesley Reading, MA, 1994).
[5] R. C. Dorf and R. H. Bishop, (1998).
[6] Y. Kuang, *Delay differential equations: with applications in population dynamics*, Vol. 191 (Academic press, 1993).
[7] M. C. Mackey and L. Glass, Science **197**, 287 (1977).
[8] O. V. Popovych, S. Yanchuk, and P. A. Tass, Phys. Rev. Lett. **107**, 228102 (2011).
[9] S. Boudkkazi, E. Carlier, N. Ankri, O. Caillard, P. Giraud, L. Fronzaroli-Molinieres, and D. Debanne, Neuron **56**, 1048 (2007).
[10] S.-N. Chow, J. Hale, and W. Huang, Proc. R. Soc. Edinburgh Sec. A **120**, 223 (1992).
[11] S. Yanchuk and P. Perlikowski, Phys. Rev. E **79**, 046221 (2009).
[12] C. R. Williams, F. Sorrentino, T. E. Murphy, and R. Roy, Chaos **23**, 043117 (2013).
[13] M. Faggian, F. Ginelli, F. Marino, and G. Giacomelli, Phys. Rev. Lett. **120**, 173901 (2018).
[14] G. Giacomelli, F. Marino, M. A. Zaks, and S. Yanchuk, Eur. Phys. Lett. **99**, 58005 (2012).
[15] L. Larger, B. Penkovsky, and Y. Maistrenko, Phys. Rev. Lett. **111**, 054103 (2013).
[16] J. D. Hart, D. C. Schmadel, T. E. Murphy, and R. Roy, Chaos **27**, 121103 (2017).
[17] J. D. Hart, L. Larger, T. E. Murphy, and R. Roy, Phil. Trans. R. Soc. A **377**, 20180123 (2019).
[18] F.T. Arecchi, G. Giacomelli, A. Lapucci, and R. Meucci, Phys. Rev. A **45**, R4225 (1992).
[19] J. D. Farmer, Physica D: **4**, 366 (1982).
[20] A. Otto, W. Just, and G. Radons, Phil. Trans. R. Soc. A **377**, 20180389 (2019).
[21] D. Senthilkumar and M. Lakshmanan, Chaos **17**, 013112 (2007).
[22] G. Radons, H.-L. Yang, J. Wang, and J.-F. Fu, Eur. Phys. J. B **71**, 111 (2009).
[23] S. Madruga, S. Boccaletti, and M. A. Matias, Int. J. Bifurc. Chaos **11**, 2875 (2001).
[24] A. Otto and G. Radons, CIRP Journal of Manufacturing Science and Technology **6**, 102 (2013).
[25] Y. Sugitani, K. Konishi, and N. Hara, Nonlinear Dynamics **70**, 2227 (2012).
[26] T. Jüngling, A. Gjurchinovski, and V. Urumov, Phys. Rev. E **86**, 046213 (2012).
[27] D. Müller, A. Otto, and G. Radons, Phys. Rev. Lett. **120**, 084102 (2018).
[28] X. S. Yao and L. Maleki, JOSA B **13**, 1725 (1996).
[29] L. Maleki, Nat. Photon. **5**, 728 (2011).
[30] L. Larger, M. C. Soriano, D. Brunner, L. Appeltant, J. M. Gutiérrez, L. Pesquera, C. R. Mirasso, and I. Fischer, Opt. Exp. **20**, 3241 (2012).
[31] Y. Paquot, F. Duport, A. Smerieri, J. Dambre, B. Schrauwen, M. Haelterman, and S. Massar, Sci. Rep. **2**, 287 (2012).
[32] J. Yao, J. of Light. Technol. **35**, 3489 (2017).
[33] A. Argyris, D. Syvridis, L. Larger, V. Annovazzi-Lodi, P. Colet, I. Fischer, J. Garcia-Ojalvo, C. R. Mirasso, L. Pesquera, and K. A. Shore, Nature **438**, 343 (2005).
[34] T. E. Murphy, A. B. Cohen, B. Ravoori, K. R. Schmitt, A. V. Setty, F. Sorrentino, C. R. Williams, E. Ott, and R. Roy, Phil. Trans. R. Soc. A **368**, 343 (2010).
[35] L. Larger and J. M. Dudley, Nature **465**, 41 (2010).
[36] L. Larger, Phil. Trans. R. Soc. A **371**, 20120464 (2013).
[37] Y. C. Kouomou, P. Colet, L. Larger, and N. Gastaud, Phys. Rev. Lett. **95**, 203903 (2005).
[38] K. E. Callan, L. Illing, Z. Gao, D. J. Gauthier, and E. Schöll, Phys. Rev. Lett. **104**, 113901 (2010).
[39] A. Otto, D. Müller, and G. Radons, Phys. Rev. Lett. **118**, 044104 (2017).
[40] D. Müller, A. Otto, and G. Radons, Phys. Rev. E **95**, 062214 (2017).
[41] G. Stepan, J. G. Milton, and T. Insperger, Chaos **27** (2017).
[42] J. G. Milton, T. Insperger, W. Cook, D. M. Harris, and G. Stepan, Phys. Rev. E **98**, 022223 (2018).
[43] D. Müller-Bender, A. Otto, and G. Radons, Phil. Trans. R. Soc. A **377**, 20180119 (2019).
[44] J. Martínez-Llinàs, P. Colet, and T. Erneux, Phys. Rev. E **91**, 032911 (2015)